J|A|C|S
ARTICLES
Published on Web 06/02/2004

Polymer Microgels: Reactors for Semiconductor, Metal, and Magnetic Nanoparticles

Jiguang Zhang, Shengqing Xu, and Eugenia Kumacheva*

Contribution from the Department of Chemistry, University of Toronto, 80 St. George Street, Toronto, Ontario, M5S 3H6, Canada

Received December 4, 2003; E-mail: ekumache@chem.utoronto.ca

Abstract: We report a strategy for the production of materials with structural hierarchy. The approach employs polymer microgels as templates for the synthesis of semiconductor, metal, or magnetic nanoparticles (NPs). We show that NPs with predetermined dimensions and size-dependent properties can be synthesized by using a very delicate balance between the reaction conditions, the composition and the structure of microgel templates, and the concentration of NPs in the microgel. Postheat treatment of microgels doped with semiconductor nanoparticles reduces NP polydispersity and allows control of their photoluminescence. Microgel templates are particularly beneficial in the synthesis of polymer microspheres heavily loaded with monodisperse superparamagnetic Fe_3O_4 NPs. Hybrid submicrometer-size microgels have promising potential applications in photonics, catalysis, and separation technologies.

Introduction

Over the past decade, inorganic nanoparticles, NPs, showed promising applications in electronic and optical devices, magnetic recording media, biological labeling, catalysis, and quantum computing.[1,2] Submicrometer-size colloid particles (comprehensively studied in the past 40 years) have attracted revived interest due to their potential applications in photonic crystals, sensors, immunoassays, and bioseparation.[3] More recently, systems with structural hierarchy, combining nanometer and submicrometer characteristic length scales, have received considerable attention. Polymer microbeads doped with luminescent NPs were used for biological labeling.[4] Photonic crystals obtained from microspheres coated with semiconductor NPs showed coupling of structurally and angularly dependent electromagnetic resonances (arising from microscale structural periodicity) and optical properties of quantum dots (providing spectral control through the quantum confinement effect).[5] The incorporation of magnetic NPs in microspheres assisted colloid crystallization of the latter under the action of magnetic field.[6] Metallodielectric microspheres showed tunable surface plasmon properties.[7] Colloid crystals produced from polymer microgels doped with metal NPs were used for the patterning of self-assembled photonic materials.[8]

The incorporation of preformed inorganic NPs into the interior of microspheres generally does not allow one to achieve a high concentration of NPs;[6] it often leads to the change in NP properties,[9] and it may result in aggregation of NPs and/or microbeads.[9,10] In-situ synthesis of nanoparticles in the interior of the microspheres (that is, template-based synthesis) is an alternative approach to this procedure. We stress that in-situ synthesis of NPs in microbeads such as ion-exchange resins,[11] latex spheres,[12] or microgels[13−15] has a two-fold advantage: the use of polymer spheres as the microreactors and the production of a material with structural hierarchy.

(1) (a) Lieber, C. M. *MRS Bull.* **2003**, *28*, 486-491. (b) Alivisatos, A. P. *Science* **1996**, *271*, 933−937. (c) Murray, C. B.; Norris, D. J.; Bawendi, M. G. *J. Am. Chem. Soc.* **1993**, *115*, 8706−8715.
(2) (a) Bruchez, M., Jr.; Moronne, M.; Gin, P.; Weiss, S.; Alivisatos, A. P. *Science* **1998**, *281*, 2013−2016. (b) Chan, W. C. W.; Nie, S. M. *Science* **1998**, *281*, 2016−2018. (c) Winter, J. O.; Liu, T. Y.; Korgel, B. A.; Schmidt, C. E. *Adv. Mater.* **2001**, *13*, 1673−1677. (d) Dubertret, B.; Skourides, P.; Norris, D. J.; Noireaux, V.; Brivanlou, A. H.; Libchaber, A. *Science* **2002**, *298*, 1759−1762. (e) Moeser, G. D.; Roach, K. A.; Green, W. H.; Laibinis, P. E. *Ind. Eng. Chem. Res.* **2002**, *41*, 4739−4749.
(3) (a) Wijnhoven, J. E. G. J.; Vos, W. L. *Science* **1998**, *281*, 802−804. (b) Holland, B. T.; Blanford, C. F.; Stein, A. *Science* **1998**, *281*, 538−540. (c) Imhof, A.; Pine, D. J. *Nature* **1997**, *389*, 948−951. (d) Li, Y. Y.; Cunin, F.; Link, J. R.; Gao, T.; Betts, R. E.; Reiver, S. H.; Chin, V.; Bhatia, S. N.; Sailor, M. J. *Science* **2003**, *299*, 2045−2047.
(4) Han, M.; Gao, X.; Su, J. Z.; Nie, S. *Nat. Biotechnol.* **2001**, *19*, 631−635.
(5) (a) Blanco, A.; López, C.; Mayoral, R.; Míguez, H.; Meseguer, F.; Mifsud, A.; Herrero, *J. Appl. Phys. Lett.* **1998**, *73*, 1781−1783. (b) Vlasov, Yu. A.; Luterova, K.; Pelant, I.; Hönerlage, B.; Astratov, V. N. *Appl. Phys. Lett.* **1997**, *71*, 1616−1618. (c) Rogach, A.; Susha, A.; Caruso, F.; Sukhorukov, G.; Kornowski, A.; Kershaw, S.; Mohwald, H.; Eychmuller, A.; Weller, H. *Adv. Mater.* **2000**, *12*, 333−337. (d) Lin, Y.; Zhang, J.; Sargent, E. H.; Kumacheva, E. *Appl. Phys. Lett.* **2002**, *81*, 3134−3136.
(6) Xu, X. L.; Majetich, S. A.; Asher, S. A. *J. Am. Chem. Soc.* **2002**, *124*, 13864−13868.
(7) Oldeburg, S. J.; Averitt, R. D.; Westcott, S. L.; Halas, N. *Chem. Phys. Lett.* **1998**, *288*, 243−247.
(8) Jones, C. D.; Lyon, L. A. *J. Am. Chem. Soc.* **2003**, *125*, 460−465.
(9) See, for example: Rogach, A. L.; Nagesha, D.; Ostrander, J. W.; Giersig, M.; Kotov, N. A. *Chem. Mater.* **2000**, *12*, 2676−2685.
(10) Coulomb interactions between microbeads and NPs suppress electrostatic stabilization of microbeads, which results in their aggregation (unpublished results).
(11) Ziolo, R. F.; Giannelis, E. P.; Weinstein, B. A.; O'Horo, M.; Ganguly, B. N.; Mehrotra, V.; Russell, M. W.; Huffman, D. R. *Science* **1992**, *257*, 219−223.
(12) (a) Ugelstad, J.; Berge, A.; Ellingsen, T.; Schmid, R.; Nilsen, T.-N.; Mork, P. C.; Stenstad, P.; Hornes, E.; Olsvik, O. *Prog. Polym. Sci.* **1992**, *17*, 87−161. (b) Zhang, J.; Coombs, N.; Kumacheva, E. *J. Am. Chem. Soc.* **2002**, *124*, 14512−14513. (c) Zhang, J.; Coombs, N.; Kumacheva, E.; Lin, Y.; Sargent, E. H. *Adv. Mater.* **2002**, *14*, 1756−1759.
(13) Kroll, E.; Winnik, F. M.; Ziolo, R. F. *Chem. Mater.* **1996**, *8*, 1594−1596.
(14) (a) Xu, S.; Zhang, J.; Paquet, C.; Lin, Y.; Kumacheva, E. *Adv. Funct. Mater.* **2003**, *13*, 468−472. (b) Xu, S.; Zhang, J.; Kumacheva, E. *Compos. Interfaces* **2003**, *10*, 405−421.
(15) (a) Antonietti, M.; Grohn, F.; Hartmann, H.; Bronstein, L. *Angew. Chem., Int. Ed. Engl.* **1997**, *36*, 2080−2083. (b) Breulmann, M.; Colfen, H.; Hentze, H.-P.; Antonietti, M.; Walsh, D.; Mann, S. *Adv. Mater.* **1998**, *10*, 237−241.

10.1021/ja031523k CCC: $27.50

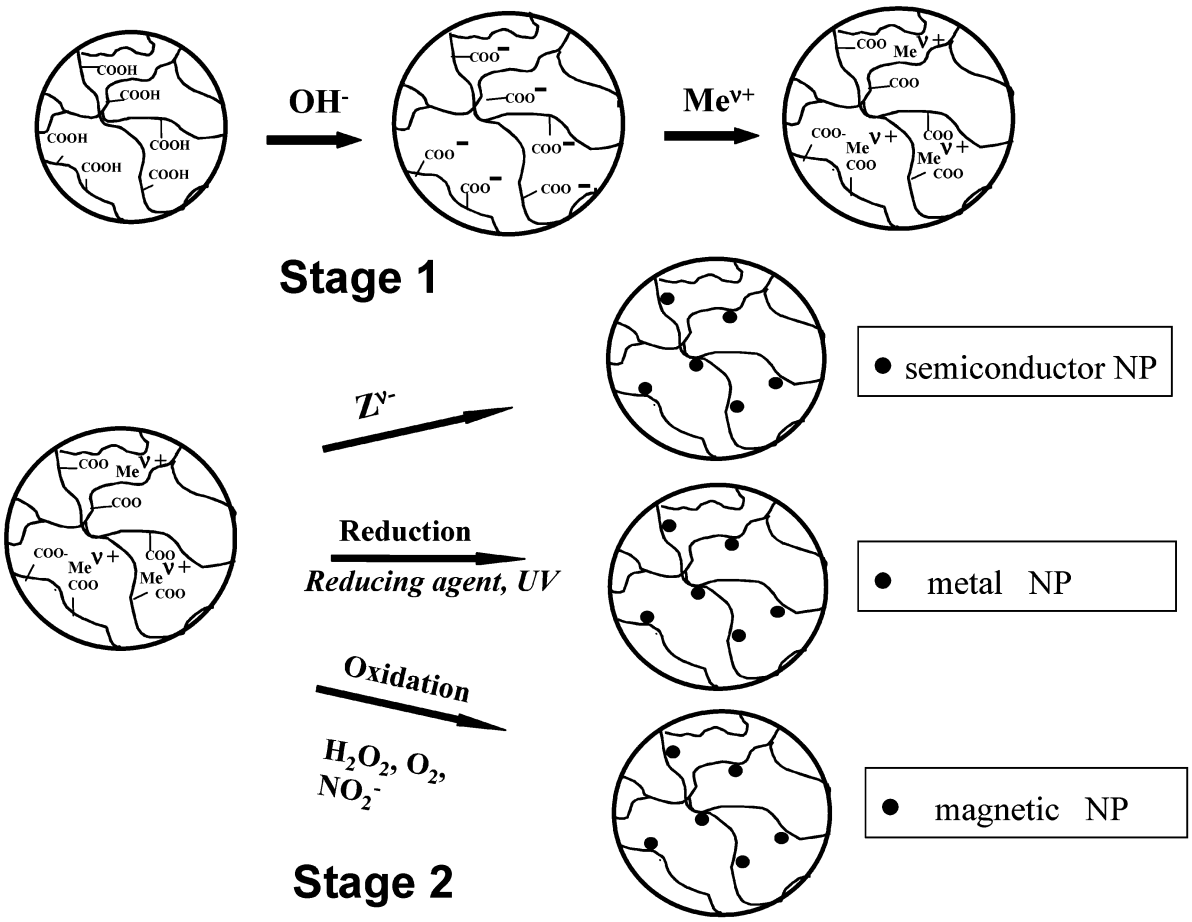

Figure 1. Schematic of microgel-based synthesis of semiconductor, metal, and magnetic nanoparticles.

While the feasibility of the synthesis of NPs in microbeads has been proven, to date, control over NP size, shape, and quality remains a synthetic challenge: in-situ synthesized NPs are generally polydispersed and/or are present in low quantities; they have surface defects and peculiar shapes. These drawbacks limit potential applications of hybrid microspheres, especially when NPs show size-dependent properties, such as absorption and luminescence[5] or magnetic properties.[16]

Here, we report the template-based synthesis of various inorganic NPs in the interior of polymer microgels. In contrast to other polymer templates, such as dendrimers,[17] block copolymer micelles,[18] and star block copolymers,[19] polymer microgels have the advantages of simple synthesis and easy functionalization. In addition, in comparison with other template systems, microgel particles may have a relatively large size, a feature important for photonic applications of hybrid microgels. The main advantages of microgels, however, originate from their network structure: (i) each void can be used for NP nucleation and growth; (ii) microgels undergo volume transitions in response to external stimuli (e.g., temperature, pH, ionic strength, or the action of electric field); and (iii) functional species other than NPs, for example, small protein or drug molecules, can be incorporated and then released from the interior of microgels.[20]

In general, microgels can serve as the microreactors for a variety of inorganic nanoparticles. Here, we describe the synthesis of three exemplary types of NPs: semiconductor, metal, and magnetic nanoparticles. We show that a very delicate balance between the reaction conditions, the composition of microgels, and NP concentration in microgels allows one to synthesize NPs with predetermined properties. In the case of semiconductor NPs whose optical properties are size- and polydispersity-dependent, we enhanced these characteristics by postheat treatment of hybrid microgels. For microgels doped with magnetic NPs, we achieved high nanoparticle monodispersity and magnetic susceptibility, along with a large NP concentration in microgels. To the best of our knowledge, this is the first comprehensive study of the in-situ synthesis of inorganic NPs in microgel templates, accompanied by the demonstration of properties of hybrid systems.

Results and Discussion

Figure 1 shows a schematic of the synthetic route used in the present study. In stage 1, precursor cations were incorporated

(16) (a) *Nanomagnetism*; Hernando, A., Ed.; Kluwer Academic Publishers: Dordrecht, The Netherlands, 1993. (b) Easom, K. A.; Klabunde, K. J.; Sorenson, C. M.; Hadjipanayis, G. C. *Polyhedron* **1994**, *13*, 1197−1223.
(17) (a) Sooklal, K.; Hanus, L. H.; Ploehn, H. J.; Murphy, C. J. *Adv. Mater.* **1998**, *10*, 1083−1087. (b) Lemon, B. I.; Crooks, R. M. *J. Am. Chem. Soc.* **2000**, *122*, 12886−12887. (c) Scott, R. W. J.; Datye, A. K.; Crooks, R. M. *J. Am. Chem. Soc.* **2003**, *125*, 3708−3709.
(18) (a) Moffitt, M.; McMahon, P. V.; Eisenberg, A. *Chem. Mater.* **1995**, *7*, 1185−1192. (b) Moffitt, M.; Vali, H.; Eisenberg, A. *Chem. Mater.* **1998**, *10*, 1021−1028. (c) Zhao, H.; Douglas, E. P. *Chem. Mater.* **2002**, *14*, 1418−1423.
(19) Youk, J. H.; Park, M.; Locklin, J.; Advincula, R.; Yang, J.; Mays, J. *Langmuir* **2002**, *18*, 2455−2458.
(20) (a) Lynn, D. M.; Amiji, M. M.; Langer, R. *Angew. Chem., Int. Ed.* **2001**, *40*, 1707−1710. (b) Murthy, N.; Xu, M. C.; Schuck, S.; Kunisawa, J.; Shastri, N.; Frechet, J. M. J. *Proc. Natl. Acad. Sci. U.S.A.* **2003**, *100*, 4995−5000.

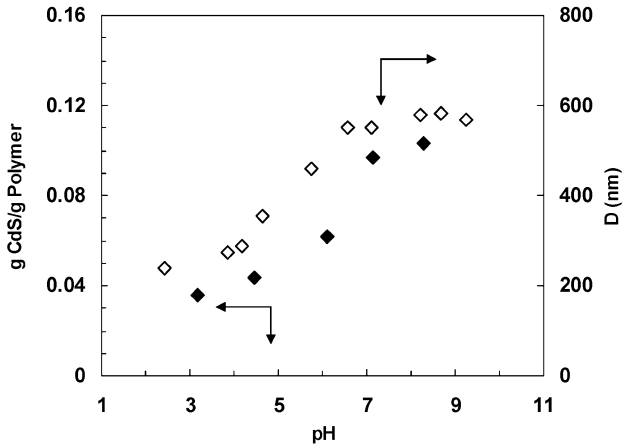

Figure 2. Variation in diameter of poly(NIPAM-AA-HEA) microgel particles (◇) and in the concentration of CdS NPs in microgel (◆) plotted versus variation in pH. Molar ratio [AA]/[HEA]/[NIPAM] is 0.36/0.13/1; $[COOH]/[Cd^{2+}]/[S^{2-}] = 1/0.5/0.5$; [BIS] = 4 mol %.

into the poly(*N*-isopropyl acrylamide-acrylic acid-2-hydroxyethyl acrylate) (poly(NIPAM-AA-HEA)) microgel particles crosslinked with *N*,*N*′-methylene bisacrylamide (BIS). The process was driven by ion exchange between the bulk solution of water-soluble salts and the interior of microgels. In the first step of stage 1, carboxyl groups of AA repeat units were deprotonated at an elevated pH. Stage 2 was determined by the type of NPs to be synthesized and is described in the Supporting Information.

Microgels with dimensions from 200 to 600 nm and a polydispersity of 4 ± 1% contained a constant molar fraction of poly(*N*-isopropyl acrylamide) at a varying molar ratio poly(acrylic acid)/poly(2-hydroxyethyl acrylate). The introduction of acrylic acid into the microgels was motivated by the need for ionizable groups interacting with metal cations. Copolymerization of *N*-isopropyl acrylamide with 2-hydroxyethyl acrylate increased microgel void size,[21] spatially separated the nucleation sites of NPs, and enhanced the compatibility of hybrid microgels with a hydrophobic shell (required in fabrication of photonic crystals).[14a] We examined three features of the template-based synthesis of NPs, all controlled by reaction conditions and the composition of microgels: the doping level of the microspheres with nanoparticles, the morphology of NPs and hybrid microgels, and the properties of NPs localized in the interior of microgels such as their structure, size distribution, polydispersity, surface characteristics, and optical and magnetic properties.

Concentration of Nanoparticles in Microgels. Effect of pH. Figure 2 shows that the increase in pH in the first step of nanoparticle synthesis (Figure 1, stage 1) led to a gradual increase in concentration of CdS NPs in the microgel. Stronger ionization of carboxyl groups of poly(acrylic acid) increased the driving force for the incorporation of cations into the microspheres. In addition, microgel size (and hence microgel voids) increased with increasing pH: in the range $2.3 < pH < 9.2$, the hydrodynamic radius of microgel particles increased from 230 to 600 nm. For poly(acrylic acid), $pK_a = 4.75$.[22] An

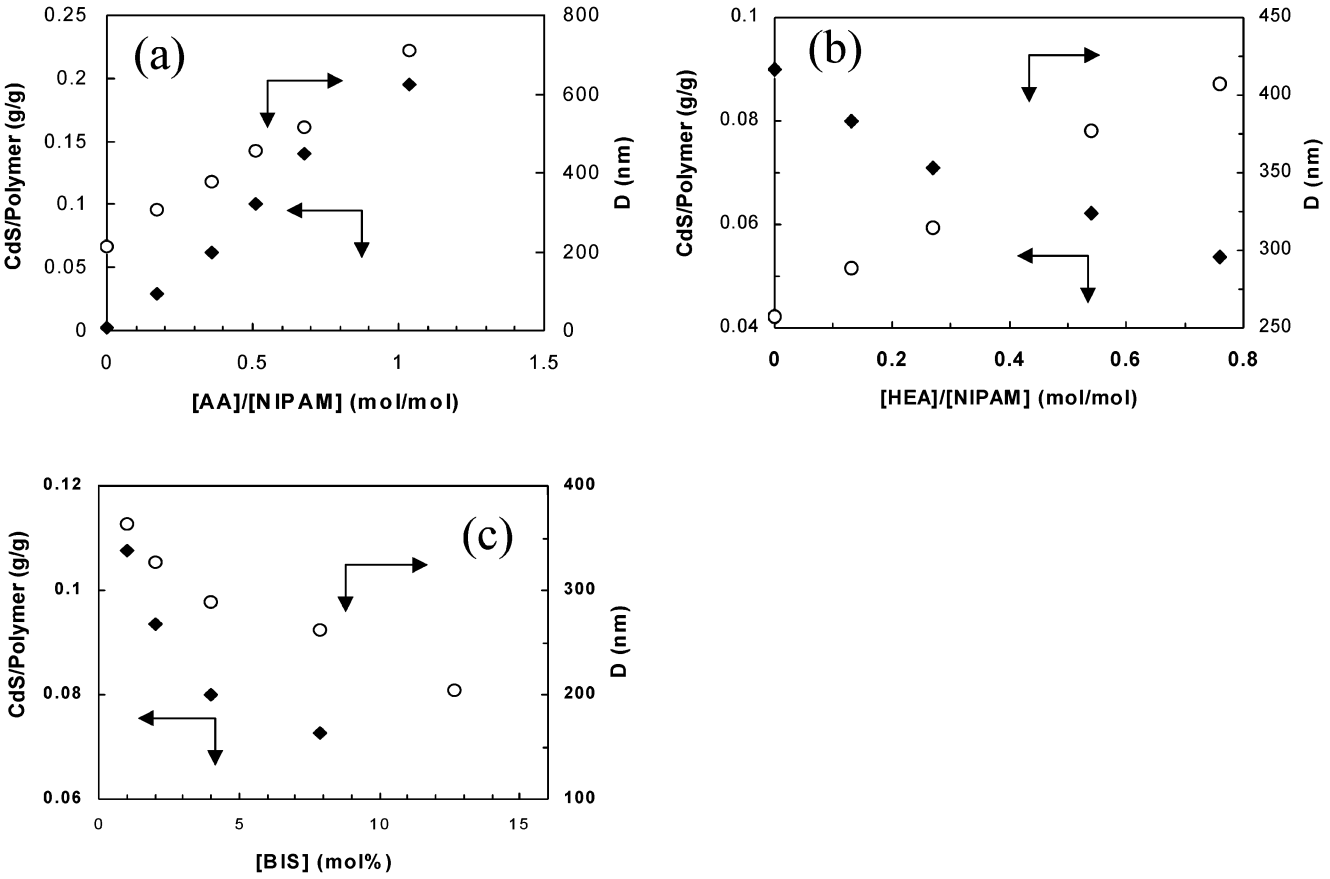

Figure 3. Variation in concentration of CdS NPs in microgels (◆) and in microgel size (○) plotted versus (a) fraction of AA in microgels for molar ratio [HEA]/[NIPAM] = 0.54; [BIS] = 4 mol %; (b) fraction of HEA in microgels for [AA]/[NIPAM] = 0.36; [BIS] = 4 mol %; (c) concentration of crosslinking agent for [AA]/[HEA]/[NIPAM] = 0.36/0.13/1. Molar ratio $[COOH]/[Cd^{2+}]/[S^{2-}]$ was 1/0.5/0.5. Microgels were ionized at pH = 8.3.

increase in microgel size occurred due to the electrostatic repulsion between the COO^--groups and the change in the conformation of fragments of poly(acrylic acid) from a highly compact structure to an expanded coil conformation. The range $6 < pH < 9$ was not, however, fully realized in the NP synthesis due to the formation of insoluble metal hydroxides at elevated pH. The threshold values of pH in the synthesis of CdS, Ag, and Fe_3O_4 NPs were limited by the values of the solubility products: $K_{sp,Cd(OH)_2} = 7.2 \times 10^{-15}$, $K_{sp,AgOH} = 2.0 \times 10^{-8}$, and $K_{sp\ Fe(OH)_2} = 4.87 \times 10^{-17}$, respectively.[23] For example, the upper values of pH were 8.35 for $[Cd^{2+}] = 1.5$ mM, 8.8 for $[Ag^+] = 3$ mM, and 7.1 for $[Fe^{2+}] = 1.5$ mM.

Effect of Microgel Composition and Stoichiometry. Figure 3a−c shows the variation in concentration of NPs versus the fraction of AA and HEA fragments and the amount of BIS in microgels, respectively. The variation in microgel size is given on the same graphs. Figure 3a,c shows that with an increase in the amount of AA and BIS in the microgels the variation in concentration of CdS NPs followed the trend in change of microgel size. In addition, an increase in the amount of AA in microgels increased the affinity of Cd^{2+}-ions to microgels, which in turn resulted in an increase of CdS concentration. In contrast, in Figure 3b, an increase in HEA fraction resulted in a decreased loading of microgels with CdS NPs (despite increasing microsphere size) because of the hydrophobic nature of HEA and a reduced concentration of COOH groups.

The concentration of CdS nanoparticles in the microgels was further controlled by changing the molar ratio $[Cd^{2+}]/[COOH]$ (Figure 4a). The doping level of NPs was, however, lower than the value estimated from the stoichiometric ratio $([COOH]/[Cd^{2+}] = 1/0.5)$: generally, only 77.5 ± 12.5% of carboxyl groups reacted with Cd^{2+}-cations, even when the latter were added in excess. Therefore, following the introduction of metal ions in the microgel, the dispersion was dialyzed to remove free metal ions.

Figure 4b shows the variation in concentration of CdS NPs in microgels versus the molar ratio $[S^{2-}]/[Cd^{2+}]$. For $[S^{2-}]/[Cd^{2+}] \leq 1$, the microgel doping level linearly increased with the ratio $[S^{2-}]/[Cd^{2+}]$, whereas for $[S^{2-}]/[Cd^{2+}] > 1$, no notable change in CdS loading was observed, suggesting that S^{2-}-anions added in excess did not take part in the formation of CdS NPs.

Morphology of Hybrid Microgel Particles. Figure 5a−c shows typical TEM images of hybrid microgel particles doped with CdS, Ag, and Fe_3O_4 NPs, respectively. As an example, we also show a high magnification TEM image of an individual CdS NP-doped microsphere (Figure 5d). The NPs appear as the black dots on the lighter background of the microgel beads. We found that, for all hybrid microgels, the concentration of NPs had a little effect on the stability to aggregation and polydispersity of hybrid microspheres and the distribution of NPs in the interior of microgels. However, when NPs were synthesized in a lower concentration, their polydispersity reduced. The average size of CdS NPs varied from 3 to 5 nm, consistent with NP dimensions obtained from absorption spectra and X-ray powder diffraction experiments (see below). We also

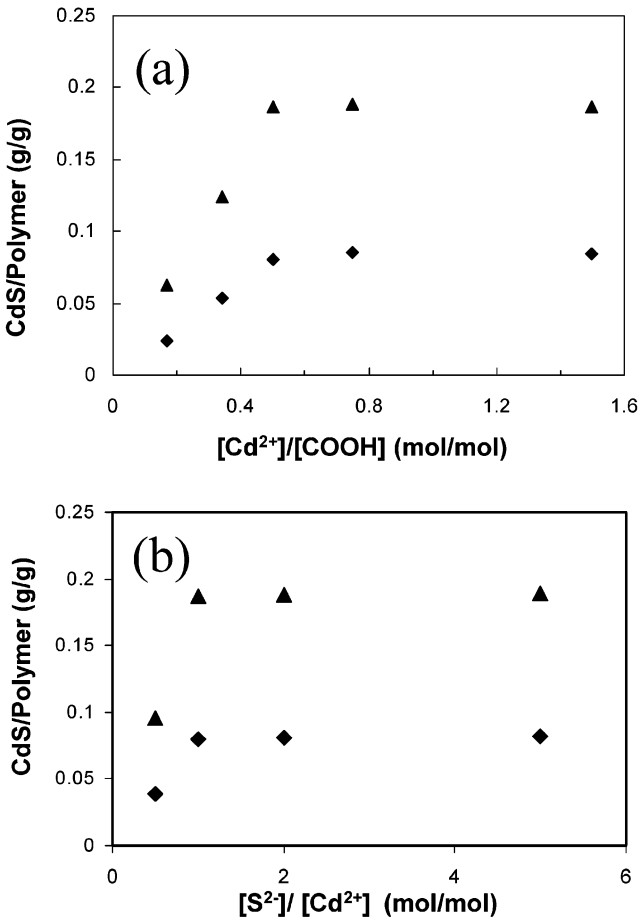

Figure 4. Variation in CdS NP concentration in microgel as a function of (a) molar ratio $[Cd^{2+}]/[COOH]$, (b) molar ratio $[S^{2-}]/[Cd^{2+}]$. Microgel composition: [AA]/[HEA]/[NIPAM] = 0.36/0.13/1, [BIS] = 4 mol % (◆); [AA]/[HEA]/[NIPAM] = 1.03/0.13/1; [BIS] = 4 mol % (▲). Microgel particles were ionized at pH = 8.3.

observed a small number of free NPs surrounding hybrid microgels. The dimensions of Ag and Fe_3O_4 NPs in microgel particles were 3 ± 1 and 8.5 ± 1.0 nm, respectively. To the best of our knowledge, the size distribution of Fe_3O_4 NPs obtained in the present work is among the best reported in the literature.[24]

The dispersions of nanoparticle-doped microgels did not aggregate for at least 4 months. The properties of NPs such as X-ray powder diffraction (XRD), photoluminescence, and nanoparticle distribution in hybrid microgels did not show a significant change after long-time storage (see Supporting Information). Hybrid microgel particles remained stimuli-responsive after 6 months of storage: poly(NIPAM-AA-HEA) underwent volume transitions in response to the variation in temperature.

Properties of in-Situ Synthesized Nanoparticles. Crystalline Structure of NPs. The structures of CdS and Fe_3O_4 NPs synthesized in the interior of microgels were characterized using XRD. In Figure 6, the top XRD pattern of CdS NPs exhibits characteristic peaks at scattering angles (2θ) of 26.4°, 43.9°, and 51.9°, corresponding to scattering from the (111), (220),

(21) Breulmann, M.; Davis, S. A.; Mann, S.; Hentze, H.-P.; Antonietti, M. *Adv. Mater*. **2000**, *12*, 502−507.
(22) *Encyclopedia Polym. Sci. Eng*., 2nd ed.; Kroschwitz, J. I., Ed.; John Wiley and Sons: New York, 1985; p 212.
(23) *Lang's Handbook of Chemistry*, 15th ed.; Dean, J. A., Ed.; McGraw-Hill: New York, 1999; Section 8.
(24) (a) Rabelo, D.; Lima, E. C. D.; Reis, A. C.; Nunes, W. C.; Nivak, M. A.; Garg, V. K.; Oliveira, A. C.; Morais, P. C. *Nano Lett*. **2001**, *1*, 105−108. (b) Wormuth, K. *J. Colloid Interface Sci.* **2001**, *241*, 366−377. (c) Lindlar, B.; Boldt, M.; Eiden-Assmann, S.; Maret, G. *Adv. Mater*. **2002**, *14*, 1656−1858.

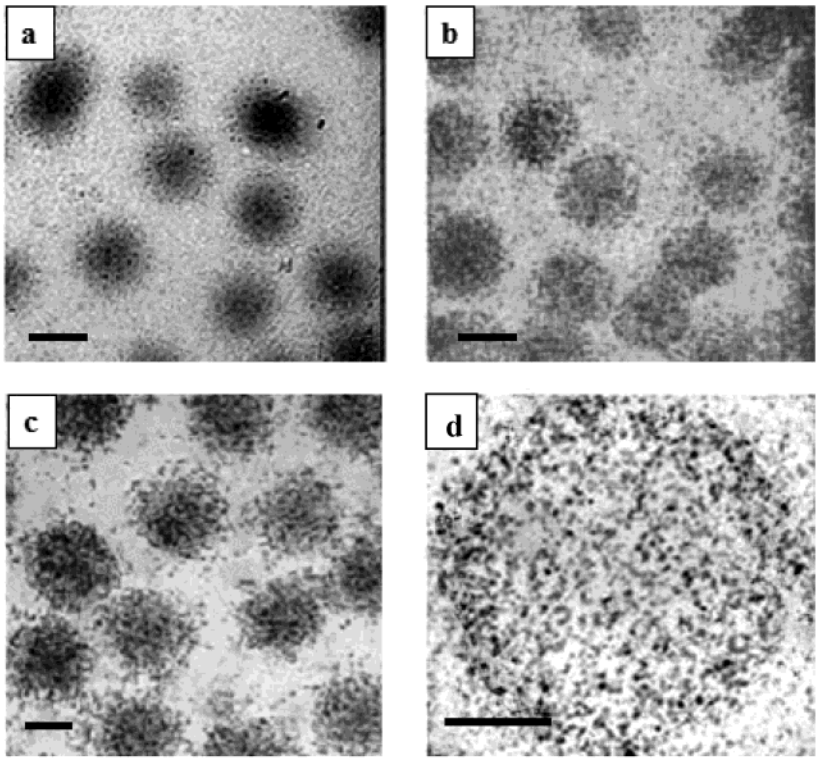

Figure 5. TEM images of hybrid poly(NIPAM-AA-HEA) microgels carrying (a) CdS; NP concentration is 0.027 g/g polymer; (b) Ag, NP concentration is 0.23 g/g polymer, (c) Fe_3O_4, NP concentration is 0.618 g/g polymer. Scale bar is 150 nm. (d) Single microgel particle doped with CdS nanocrystals. Scale bar is 50 nm.

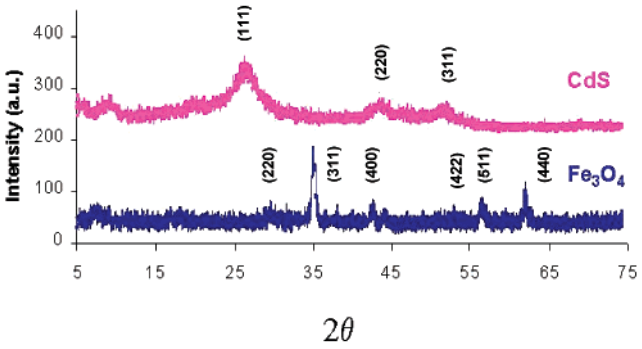

Figure 6. X-ray powder diffraction patterns of microgels doped with CdS (top) and Fe_3O_4 (bottom) NPs. Microgel compositions: [AA]/[HEA]/[NIPAM] = 0.36/0.13/1, [BIS] = 4 mol %; [COOH]/[Cd^{2+}]/[S^{2-}] = 1/0.5/0.5. CdS concentration in microgel is 0.027 g/g polymer; Fe_3O_4 concentration in microgel is 0.724 g/g polymer.

and (311) planes, respectively, of a cubic CdS crystal lattice (the standard card JCPDS file # 10-0454). The average nanocrystal size calculated using the Scherrer equation[25] was 3.1 nm, consistent with the results obtained for the same sample from TEM image analysis. Broadening of the diffraction peaks occurred due to the small NP size. The bottom pattern in Figure 6 shows the XRD spectrum for Fe_3O_4 NPs. Because the XRD patterns of magnetite (Fe_3O_4, JCPDS file #88-0315) and maghemite (γ-Fe_2O_3, JCPDS file #39-1346) are similar, they can be identified by comparing relative peak intensities. The data suggested that the nanocrystals synthesized in microgel templates were Fe_3O_4 NPs. We assigned the measured peak positions at their relative intensities (30.07° (28), 35.44° (100), 43.06° (20), 56.93° (25), and 62.64° (34)) to the (220), (311), (400), (511), and (440) planes of Fe_3O_4 lattice, respectively. The mean crystallite size was 8.1 nm,[25] in agreement with TEM image analysis.

Optical Properties of CdS and Ag NPs. We studied the optical properties of CdS and Ag nanoparticles synthesized in the interior of microgels with a two-fold purpose. First, we examined the absorption and photoluminescence of NPs to characterize their size and polydispersity. Second, with an eye on photonic applications of particles with structural hierarchy, we tested the optical properties of hybrid microgels.

Figure 7a shows the absorption spectra of CdS NPs in the interior of microgels. Increased loading of microgels with nanoparticles led to the red-shift in absorption onset from 430 to 500 nm, indicating an increase in NP size. Nevertheless, in all samples, the onset of absorption was below 510 nm (measured for bulk CdS), suggesting that the quantum confinement effect was preserved. On the basis of the NP size-absorption onset relation,[18,26] the size of the CdS nanoparticles was estimated to vary from 3.0 to 5.9 nm, similar to the results of TEM image analysis.

The dispersions of hybrid microgels doped with CdS NPs were refluxed for 12 h to refine the crystalline structure of NPs and to improve their size distribution.[27] In Figure 7a, the corresponding absorption spectra (dotted lines) measured after heat processing show a sharper onset of absorption and the appearance of absorption peaks. Both effects indicated an

(25) *X-ray Diffraction Procedures*; Klug, H. P., Alexander, L. E., Eds.; John Wiley: New York, 1959.

(26) Spanhel, L.; Haase, M.; Weller, H.; Henglein, A. *J. Am. Chem. Soc.* **1987**, *109*, 5649−5655.

(27) Vossmeyer, T.; Katsikas, L.; Giersig, M.; Popovic, I. G.; Diesner, K.; Chemseddine, A.; Eychmuller, A.; Weller, H. *J. Phys. Chem.* **1994**, *98*, 7665−7673.

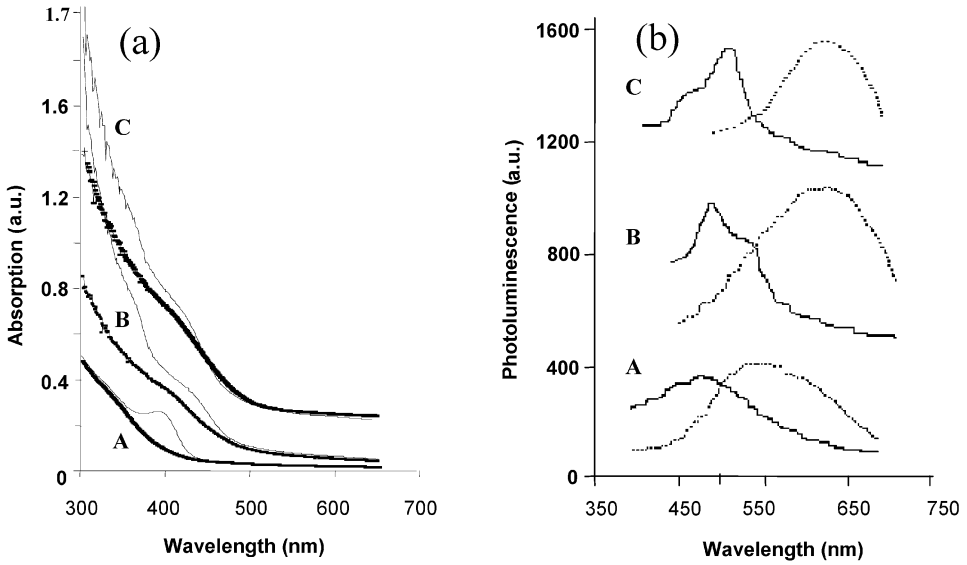

Figure 7. (a) UV−visible absorbance and (b) photoluminescence spectra of CdS NPs synthesized in microgels before (—) and after heat processing (- - - - -). [AA]/[HEA]/[NIPAM] = 0.36/0.13/1, [BIS] = 4 mol %; [COOH]/[Cd^{2+}]/[S^{2-}] = 1/0.5/0.5. From top to bottom, CdS concentration in microgels is 0.027 (A), 0.054 (B), and 0.08 (C) g/g polymer. A rising baseline characteristic of semiconductor nanoparticles obscures absorption data at wavelengths significantly lower than the absorption maximum. λ_{ex} = 380 nm.

enhanced NP size distribution caused by Ostwald ripening of smaller nanoparticles during heat processing of the system. We note that such an enhancement was stronger for hybrid microgels doped with a lower amount of CdS NPs.

Figure 7b shows the photoluminescence (PL) spectra of CdS NPs in the interior of the microgels. The PL emission bands (bottom to top, solid lines) red-shifted, and their intensity increased with increasing NP concentration in microgels. For higher NP doping levels, each PL spectrum featured two well-resolved peaks. The shorter wavelength emission bands were ascribed to band gap PL of CdS NPs, because they coincided with absorption onset of the corresponding samples in Figure 7a. The emission peaks measured at longer wavelengths resulted from the interstitial sulfur or cadmium vacancies.[28] The relative intensity of the two peaks changed with an increase in NP concentration and size. The width of the PL bands of ca. 100−160 nm was similar or only slightly broader than that measured for the CdS NPs synthesized using dendrimers,[17] linear and branched polymer stabilizers,[18,29] and block copolymer micelles[17] (but inferior to the properties of CdS NPs synthesized using a TOPO/TOP method).[30]

The PL emission bands of CdS NPs showed a notable red-shift after heat treatment of hybrid microgels (Figure 7b, dotted spectra). For microgels with a low concentration of NPs, the PL peak shifted from 485 to 566 nm and the color of microgel changed from blue to yellow. The PL emission bands of hybrid microgels with a higher concentration of CdS NPs after heat processing each featured a single broad PL peak (at ca. 620 and 690 nm). Because postheat processing of hybrid microgels improved NP size distribution (Figure 7a), we ascribe these emission bands to the recombination of electrons trapped in a sulfur vacancy with a hole in the valence band of CdS.[31] The color of these microgels after refluxing turned from blue to orange or red. Thus, by changing the NP concentration in microgels and by using postheat treatment, we obtained hybrid microgels with PL properties tunable in the entire visible spectral range. We note that no changes occurred in the crystalline structure of CdS NPs and their distribution in hybrid microgels: the XRD spectrum and the TEM image of CdS-doped microgels were similar to those given in Figures 5 and 6, respectively.

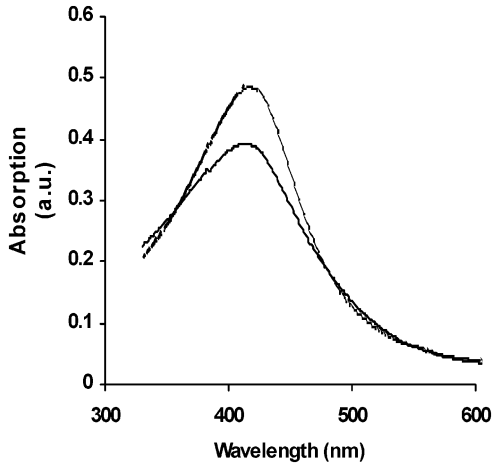

Figure 8. UV−visible absorbance spectra of Ag NPs synthesized in the interior of microgels. Ag NP concentration in microgel: 0.23 g/g polymer (bottom spectrum), 0.39 g/g polymer (top spectrum). Microgel composition is as in Figure 7.

Figure 8 shows the absorption spectra of Ag NPs in the interior of the microgels. A well-defined surface plasmon resonance was measured at 411 nm (bottom spectrum), similar to that measured for ca. 2.5 nm-size Ag NPs by Asher et al.[32] In microspheres with a lower concentration of Ag NPs (or smaller NP size), the absorption peak broadened due to the "intrinsic size effect" in metal NPs.[33]

(28) Lambe, J. J.; Klick, C. C. *Phys. Rev.* **1956**, *103*, 1715−1720.
(29) Limin Qi, L.; Cölfen, H.; Antonietti, M. *Nano Lett.* **2001**, *1*, 61−65.
(30) Peng, Z. A.; Peng, X. *J. Am. Chem. Soc.* **2001**, *123*, 183−184.
(31) (a) Chrysochoos, J. *J. Phys. Chem.* **1992**, *96*, 2868−2873. (b) Ramsden, J. J.; Webber, S. E.; Gratzel, M. J. *J. Phys. Chem.* **1985**, *89*, 2740−2743.
(32) Wang, W.; Asher, S. A. *J. Am. Chem. Soc.* **2001**, *123*, 12528−12535.
(33) Mulvaney, P. *Langmuir* **1996**, *12*, 788−800.

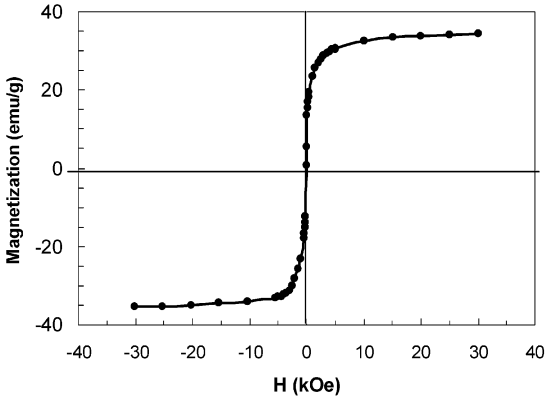

Figure 9. Magnetic properties of Fe_3O_4 NPs in the interior of dried poly(NIPAM-AA-HEA) microgel. NP concentration is 0.724 g/g polymer. T = 300 K. Microgel composition is as in Figure 7.

Magnetic Properties of Fe_3O_4 NP-Doped Microgels. Figure 9 demonstrates the magnetic properties of Fe_3O_4 NPs synthesized in the interior of 500 nm-size poly(NIPAM-AA-HEA) microgels. No hysteresis was observed in these measurements; that is, both remanence and coercivity were zero, consistent with superparamagnetic properties of magnetite NPs with a diameter below 12 nm.[16] At 10 kOe, the composite particles had a magnetic saturation moment of $Ms = 32.4$ emu/g, corresponding to a magnetic susceptibility of $\chi = 3.24 \times 10^{-3}$ emu/(g Oe) or $\chi = 0.07$ (calculated from the density of bulk magnetite of 5.18 g/cm^3).[16] Using $Ms = 92$ emu/g of the bulk magnetite,[16] we estimated the magnetic saturation moment to be $Ms = 38.6$ emu/g, higher than the experimental value of $Ms = 32.4$ emu/g. The decrease in the magnetic saturation moment was due to the small NP size.[11,16]

We stress that the synthesis of superparamagnetic Fe_3O_4 NPs in the microgel templates was extremely efficient: for NP concentration as high as 0.724 g/g polymer, the nanoparticles had an average size of ca. 8.1 nm, low polydispersity, and showed excellent magnetic properties, while the microspheres carrying these NPs remained stimuli-responsive.

In conclusion, we showed that semiconductor, metal, and magnetic NPs with predetermined size, polydispersity, and optical and magnetic properties can be successfully synthesized using polymer microgels as a template. The properties of nanoparticles are controlled by the composition and the structure of microgels and the preparation conditions. We showed that subsequent heat treatment of microgels doped with semiconductor NPs enhances nanoparticle size distribution and allows one to tune their PL emission over the entire visible spectral range. Using microgels as the templates, we synthesized very small and monodisperse Fe_3O_4 NPs with superparamagnetic properties. Hybrid microspheres reported in the present study have promising applications in catalysis, biolabeling, chemical and biological separation, and the fabrication of polymer-based materials for photonic applications.[14,34]

Acknowledgment. We gratefully acknowledge the financial support of Nortel Networks and NSERC Canada. E.K. thanks Canada Research Chair funding and the Premier Research Excellence Award. We thank Professor R. H. Pelton (McMaster University) for his initial assistance in microgel synthesis.

Supporting Information Available: Experimental details (PDF). This material is available free of charge via the Internet at http://pubs.acs.org.

JA031523K

(34) (a) Kumacheva, E.; Kalinina; O.; Lilge L. *Adv. Mater.* **1999**, *11*, 231−234. (b) Siwick, B.; Kalinina, O.; Kumacheva, E.; Miller, D. R. J. *J. Appl. Phys.* **2001**, *90*, 5328−5334. (c) Pham, H.; Gourevich, I.; Oh, J.; Jonkman, J.; Kumacheva, E. *Adv. Mater.* **2004**, *16*, 516−520.